SIS DEAD LAYER THICKNESSES

ACE Memo ID: 1998.01.30.BLD (JPL/SIS/dead layers)

From: Brian L. Dougherty (bld@heag1.jpl.nasa.gov)

To: CRIS/SIS Data Analysis Teams

Date: 30 Jan. 1998

re: This report summarizes the alpha-particle measurement methods and results.

1. Introduction

Within energy ranges of interest to SIS, the stopping power for nuclei in silicon varies as $dE/dx \equiv S \propto Z^2(E/M)^{-0.7}$; i.e. $Z^2M^{0.7}L\sec\theta \propto E^{1.7} - E'^{1.7}$ for particles that penetrate a detector of thickness L at angle θ, where E and E' are the incident and remaining energies. Therefore, mass resolutions are related to thickness uncertainties as $0.7\partial M/M \approx \partial L/L$. To achieve a 3-sigma separation of iron isotopes (yielding over 99 % discrimination) using a 100 μm detector implies its active and dead-layer depths must be known to within ~1/4 μm silicon equivalent (or ~60 $\mu g/cm^2$).

Total silicon-wafer thicknesses were measured independently and with fine accuracy using optical interferometry. For details, refer to Mark Wiedenbeck's work.

Surface dead layers are associated with the implanted contacts. The detector manufacturer (Micron Semiconductor Ltd. in the U.K.) claims the junction/ohmic sides are implanted with boron/arsenic to depths of 0.5/1 micron, and both faces have about 0.2 ± 0.1 μm of aluminum deposited on them. This represents a few percent of the range of a typical, radio-emitted alpha particle; a 6 MeV alpha loses about 130 keV going through 1 μm of silicon. Such decrements are easily discernible using these detectors and their associated electronics. Therefore, careful measurements of alpha energy losses can establish dead layer thicknesses.

2. Measurement Scheme

We measure the residual energy (E') of a set of well-known, normal-incidence alphas. Given the stopping power (S) and the incident energy (E), we then derive the dead-layer thickness (L). We assume constant stopping power; i.e. $E = E' + SL$, with $E' = m(C - b)$, where C is the mean ADC channel number of the observed alpha peak, m is the electronics conversion gain, and b is the ADC offset.

We make absolute dead-layer measurements of L with a collimated 0.2 μCi ^{228}Th source pointed at the centers of every aluminum electrode. Relative-thickness maps of ΔL are made using similarly collimated 0.2 μCi ^{244}Cm sources that are moved across the detector surfaces to 103 specified grid points. A combined look at both types of spectra is shown in Figure 1. The geometry of our setup is shown in Figure 2, and the grid is shown in Figure 3. Our 4π/350 steradian collimators produce alpha spots of maximum radius ≈ 3.4 mm. The triangular grid spacing is 9 mm, so all measurements are independent, and about 45 % of the detector surface area is sampled. Thorium data include 2 pulser peaks, and runs last 6 minutes, generating at least 4000 counts in each of 5 separate alpha peaks. Curium spectra include 1 pulser peak, and runs last 1 minute at each grid point, giving 1000 or more counts in one peak. We begin and end every ^{244}Cm scan with 1 min spectra taken at the detector center.

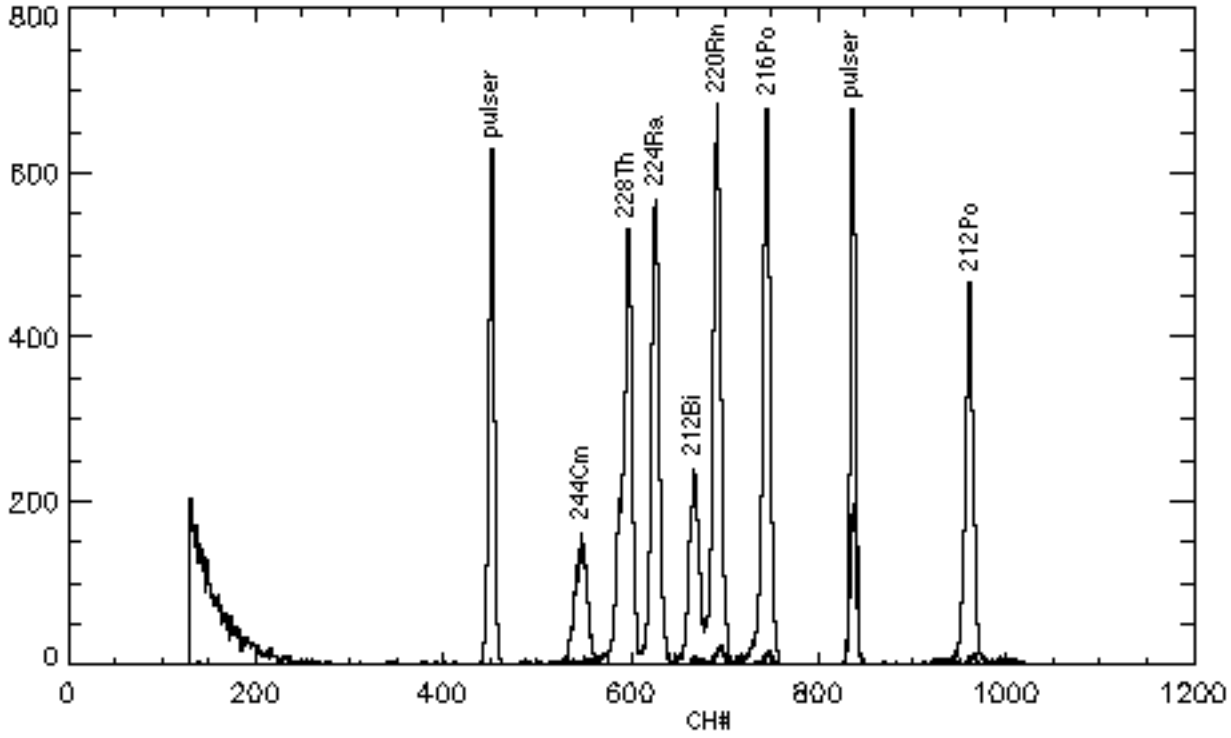

Figure 1. Sum spectrum of thorium and curium data taken at the center of detector #007.

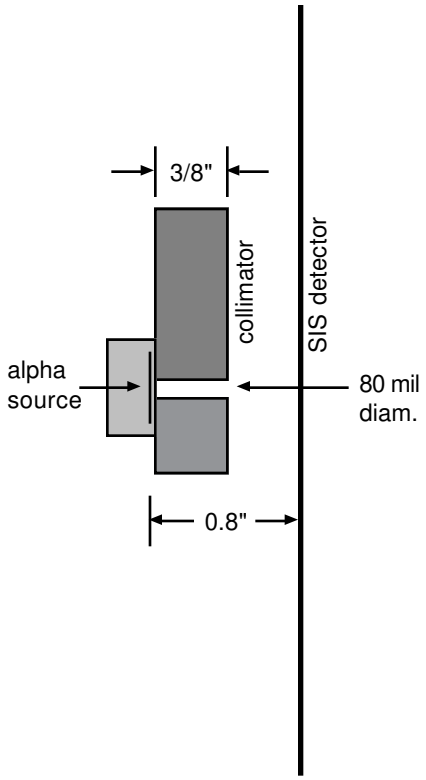

Figure 2. geometry of the measurements

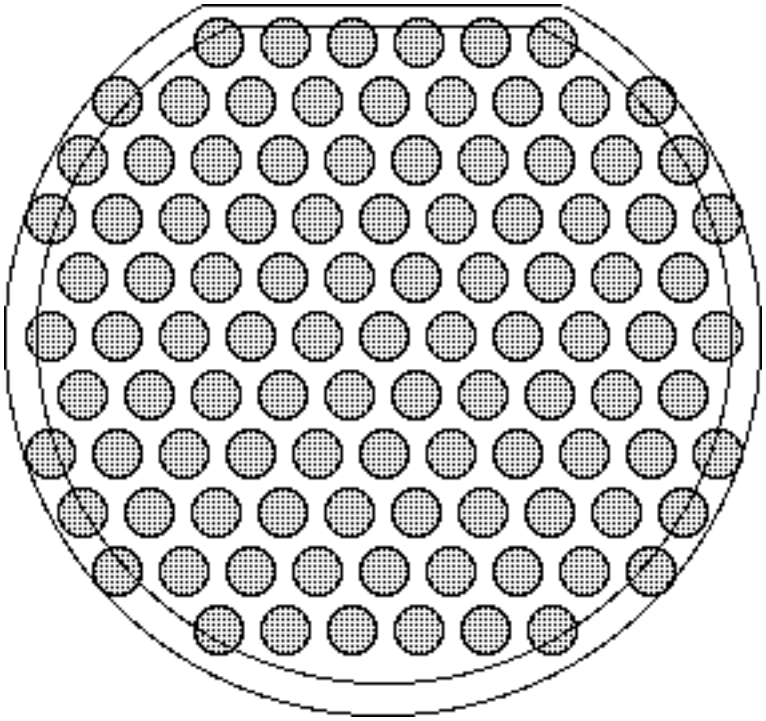

Figure 3. grid positions and alpha spot sizes

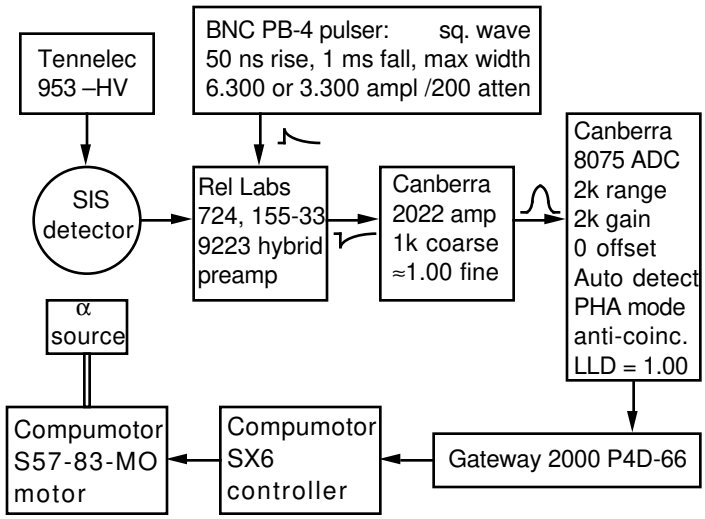

Figure 4. Electronics setup

3. General Error Analysis

Our electronics gain is subject to random uncertainties which would dominate the error in a calculation of L if we simply used the formula $SL = E - mX$ as is, where $X = C - b$. We eliminate m and avoid this problem by comparing two alpha lines from the same source. Systematic uncertainties in other quantities then dominate the error. For relative thickness measurements of ΔL, we compare ^{244}Cm alpha peak positions found at various grid points to that obtained at the detector center; i.e. $\Delta L = L_i - L_{center}$. Our working set of formulae are given below.

L	$= (E_1X_2 - E_2X_1)/D$		where suscripts denote two alpha lines at the same location	
$\partial L/\partial E_{12}$	$= X_{21}/D$		where $D = S_1X_2 - S_2X_1$	
$\partial L/\partial C_{12}$	$= mX_{21}/D$		where $m = (E_1S_2 - E_2S_1)/D$	
$\partial L/\partial S_{12}$	$= LX_{21}/D$			
$\partial L/\partial b$	$= (X_1 - X_2)m/D$			
ΔL	$= -(E - SL)\Delta C/SX$	$\approx -E\Delta C/SC$	for small L, and $\Delta C = C_i - C_{center} \equiv C - C'$	
$\partial\Delta L/\partial E$	$= \Delta L/(E - SL)$	$\approx \Delta L/E$	"	
$\partial\Delta L/\partial C'$	$= \Delta L/\Delta C$	$\approx E/SC$	"	
$\partial\Delta L/\partial C$	$= \Delta LX'/\Delta CX$	$\approx E/SC$	"	and small ΔC
$\partial\Delta L/\partial S$	$= \Delta LE/S(E - SL)$	$\approx \Delta L/S$	"	
$\partial\Delta L/\partial b$	$= \Delta L/X$	$\approx \Delta L/C$	"	and small b

We now consider the uncertainties inherent in each relevant term of these expressions.

E: the incident energy

Our alpha sources were fabricatred by Isotope Products. The initial alpha energies and branching fractions (BF) are tabulated below. Our authority is the Table of Isotopes, 7th edition.

parent	daughter	halflife	energy	BF	
^{244}Cm	—	18.11 y	5804.96 ± 0.05 keV	76.7 %	⎫ 5795.15 ± 0.08 keV
			5762.84 ± 0.30	23.3	⎭ combined average @ 100%
^{228}Th	—	1.91 y	5423.33 ± 0.22	72.7	
			5340.54 ± 0.15	26.7	
			5209.5 ± ?	0.4	
			5172.1 ± ?	0.2	
	^{224}Ra	3.66 d	5685.56 ± 0.15	95.0	
			5448.90 ± ?	5.0	
	^{220}Rn	55.6 s	6288.29 ± 0.10	99.9	
			5747 ± ?	0.1	
	^{216}Po	0.15 s	6778.50 ± 0.50	100	
	^{212}Bi	60.6 m	6090.09 ± 0.04	9.8	⎫ 6061.94 ± 0.03 keV
			6050.99 ± 0.03	25.2	⎭ combined average @ 35%
			5796 ± 3	0.6	
			5607 ± 3	0.4	
	^{212}Po	.30 μs	8784.37 ± 0.07	64.0	

The ^{228}Th source is over-plated with 1466 ± 57 (stat) ± 22 (syst) Å of Au. The ^{244}Cm sources are protected with 4 μm Ti foils, though the exact Ti thickness varies between the sources. We account for these coverings by incorporating decrements in the incident alpha energies. The most prominent and sufficiently separated alpha "lines" observed from the sources correspond to the energies (and nominal, mean Si stopping powers) listed here.

Th line energy (keV)	S (keV/μm)	Cm source#	energy (keV)**	S (keV/μm)
5635.44 ± 0.15 ± 2.43*	133.60	411	4969.4 ± 5.8	144.74
6003.50 ± 0.04 ± 2.38†	128.22	412	4903.0 ± 5.8	145.96
6230.87 ± 0.10 ± 2.33‡	125.13	413	4903.9 ± 5.8	145.95
6723.16 ± 0.50 ± 2.24	118.97	414	4890.9 ± 5.8	146.19
8735.91 ± 0.07 ± 1.89	99.47	416	4857.5 ± 5.8	146.82
		418	4908.6 ± 5.8	145.86

* this Ra line is typically joined below by the Th lines; i.e. it is not completely separated
† this Bi line is a weighted sum of two closely-spaced alphas
‡ this Rn line is typically joined below by the Bi lines; i.e. it is not completely separated
** All Cm lines are weighted sums of the two alphas

The first errors listed for Th are random; the second are systematic, and reflect ambiguities in source-calibration procedures, especially encapsulation thickness uncertainties. The latter lead to deviations in L which are correctable after-the-fact by using better calibration methods. We must adjust S along with E when such systematic effects are resolved, since the former is a function of the latter. The Cm errors are predominately statistical, and traceable to calibration peak widths.

Errors in calculated L or ΔL due to intervening air are avoided by making measurements in vacuum. Our working pressure is typically ≈ 50 mTorr, but pressures of just 1 Torr will reduce deviations to below 0.1 μm (Si equivalent) even for alpha flight paths of 10 cm in length.

S: the stopping power

We take stopping powers from the monograph by J. F. Ziegler: Helium Stopping Powers and Ranges in All Elemental Matter (Pergamon, 1977) in which he fits the following semi-empirical formula for electronic energy loss to the available data:

$$\left(dE/dx\right)^{-1} \;=\; \left(A_1 E^{A_2}\right)^{-1} \;+\; \left(E/A_3\right)\left[\ln\left(1 + A_4/E + A_5 E\right)\right]^{-1},$$

giving stopping power in units of keV/μm, with E measured in keV. The parameters for a few elements of interest are tabulated below.

target	A_1	A_2	A_3	A_4	A_5	A (keV/μm)	a
Al	15.07	0.6250	275400	100	0.004359	47800	0.667
Si	10.49	0.6500	246500	1788	0.004133	42400	0.667
Ti	26.89	0.5087	372800	8806	0.005948	60200	0.653
Au	18.62	0.5880	1345000	2954	0.001050	29900	0.496

For completeness, Ziegler also presents an expression for stopping due to elastic nuclear collisions, which occur along with electronic losses: but nuclear stopping is always negligible in the energy range considered here.

For alphas with energies between 5 and 9 MeV, Ziegler's formula may be approximated to within 0.3 % by the power-law relation $dE/dx \approx AE^{-a}$. Values for (A,a) are listed above, with E measured in keV. Thus, alphas of kinetic energy E incident at angle θ with respect to the normal on a dead layer of thickness L survive with energy E' as $A(1+a)L = \cos\theta\ (E^{1+a} - E'^{1+a})$ into the active detector region. Since SIS-detector dead layers are very thin, however, we can approximate the stopping as constant, with particular values of S computed for each incident alpha energy. Slight analytic errors are introduced by not using the power-law approximation; e.g. we get a tiny over-estimate of the dead layer thickness. Such (calculable) errors are partially offset by the use of exact S values ala Ziegler.

Ziegler's fits return stopping-powers that are ≤ 1 % above those found in Northcliffe and Schilling ("Range and Stopping Power Tables for Heavy Ions", *Nuclear Data Tables* **A7** 233, 1970), and 1.0 ± 0.1 % above those derived from J. Janni (Air Force Weapons Lab report TR-65-150, 1966). If all such values are physically accurate, then the small mismatches between tables and formulae represent trivial uncertainties. Unfortunately, it is impractical to measure stopping powers independently, especially to the precision required. It is also impossible to completely eliminate our dependence upon these terms in our analyses: that is, not if we wish to trade minor errors in S with large uncertainties in other factors. Thus, we are left with systematic uncertainties of up to 1 % in S. This dominates over uncertainties due to errors in the incident alpha energies from which S values are derived. We deal with this problem like we do with systematic ambiguities in E values; dead-layer deviations due to vagaries in S are correctable after-the-fact if more accurate stopping-power formulae or tabulations are found.

The dead layers are not composed purely of silicon, but include implanted dopants, possible oxide interfaces, and an overlying deposition of aluminum. But the concentrations of boron and arsenic in the crystal bulk are at most one part in a million, so their presence may be neglected: and oxide layers are likely to be insensibly thin. Furthermore, since stopping powers in aluminum are typically just 12 % higher than in silicon, we treat both materials the same, as though there is one continuous dead layer made of silicon. This introduces a small systematic over-estimate: the derived dead layer thickness will be (1 + 0.12*r) times the actual dead thickness of silicon plus aluminum, where r is the fraction of Al involved, measured in μm. However, as a way of parameterizing the total dead layer thickness, this fiat is accurate.

E'(m,b,C): the residual energy

As noted above, the conversion gain (m) is eliminated in our analyses. To understand why, suppose (1) the raw electrical gain could be established to high precision with a pulser and standard capacitor, (2) subtle differences in pulse shape between real and pulser signals did not effect the calibration, (3) small gain changes did not occasionally appear when detector bias was toggled, and (4) changes in charge collection efficiency and ballistic deficits at different grid points in a scan did not occur. We would still be left with (5) a nearly 1 % uncertainty in the literature on the average energy required to liberate each electron-hole pair for ionizing events in silicon. All these effects are systematic to some extent, and one could think of treating them the same as with similar effects in E and S. The range of corrrections anticipated is huge, however, and such ambiguities would overwhelmingly dominate other errors in our calculated dead-layer thicknesses.

Pulser peaks are used to find electronics offsets (b) in ^{228}Th data and to check for gain changes during ^{244}Cm scans. We use a relatively low-rate pulser (≈ 20 Hz) to avoid pile-up effects. The resulting peaks still have somewhat better statistics than do the observed alpha peaks. We trust that our ADCs remain linear throughout the data-taking effort.

Alpha peaks are nearly Gaussian, but significant low-side tails often appear. The latter usually occur when part of the alpha spot falls outside the diode-contact edge, where reduced electric fields and concomitant low charge collection efficiencies are present. Line shapes are fit with checking procedures to reduce sensitivities to outlying counts and to spikes. We take the usual statistical measure for the uncertainty on the mean of a spectral peak to be equal to its rms width divided by the square root of the number of counts in the peak.

θ: the angle of incidence (implicit)

The angle of incidence must be controlled, but not excessively so. A large, and obvious tilt on an otherwise normally incident beam would be needed to introduce errors comparable to the level of precision sought. Our collimators yield a mean incidence angle of ≈ 5.3°, and an rms angular spread of about 5.9°. However, the orientation of each collimator, limited by machining and positioning errors, is probably good to within ± 2° of normal. Thus, dead layer thicknesses are measured to within ≈ 0.5 %, which for L ≈ 1 μm is well below our limit of resolution.

Channelling is largely avoided since most incidence angles are not aligned with crystal axes or planes. This is confirmed by the relative absence of high-side tails on the alpha peaks.

Our collimators lead to an rms "spot" radius of ≈ 1.7 mm; i.e. most of the alphas hit our detectors within 1.7 mm of the spot centers. The total flux-weighted area sampled during a scan, therefore, is roughly 30 % of the 63.6 cm^2 active region.

4. Results

Depletion voltages were first determined by quickly scanning (with a 5 sec dwell per grid point) the ohmic surface of each detector and mapping pulse height variations for different biases. These maps showed distinctive patterns associated with incomplete activation (see Figure 5). Full depletion was declared when an approximately uniform, featureless response was obtained.

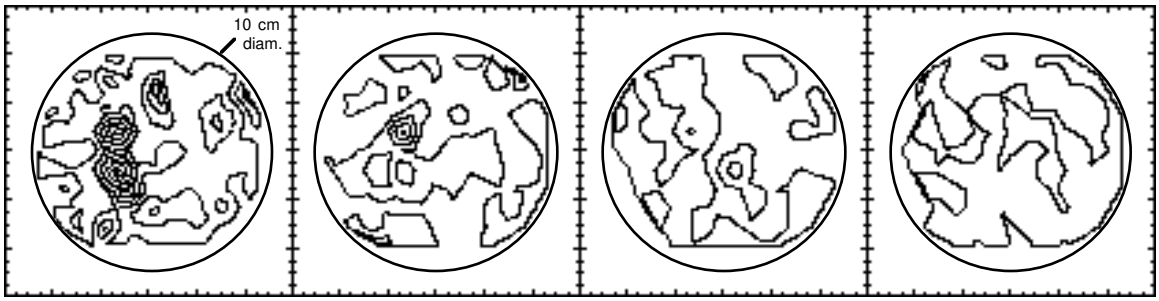

Figure 5. Contour maps of ^{244}Cm alpha particle pulse heights obtained with one 1000 μm thick detector. Contours are spaced by ≈0.6 % of full-height pulses, equivalent to a ≈0.2 μm change in dead layer thickness. The two adjoined, densely-lined hexagons near the center in (a) indicate large deficits in the collected charge (at two grid positions). These "holes", due to incomplete depletion, rapidly become shallower at 110 V in (b), and nearly disappear at 120 V in (c). Other irregularities in pulse height also improve, and the response map becomes more uniform. At 170 V in (d) the contours fluctuate near the limit of precision for these fast-scan measurements.

Higher-statistics dead-layer maps were then made with each detector biased near the voltage anticipated for flight: usually just ~10 V below breakdown for the thicker devices, or at the corresponding bias supply maximum for the thinner detectors. (Breakdowns were revealed by rapid increases of noise and/or current.) Typically, uncertainties of better than 0.03 μm rms were achieved, and dead layers generally were uniform on all surfaces. Those devices in which significant "features" remained were disfavored as possible elements in the flight stacks. Results for the flight detectors are summarized in the table below.

These results do not coincide with the nominal implantation depths indicated by Micron Semiconductor. In fact, the measured dead layers are close to those due to the putative aluminum metallizations alone. Such a finding was not expected, especially for the junction sides, where low-strength fields are present. One possibility we have considered is that the contacts are partially

"active"; i.e. some of the charge deposited in the junctions is collected in spite of the low field strength in these layers. Measurements taken at lower bias, nearer depletion, indicated a general (~23 %) thickening of the apparent dead layers on both surfaces. This is equivalent to a ~0.2 % decrement in charge collection efficiency. Losses may also be occurring in the crystal bulk (due to trapping?) in regions where there are low-strength electric fields.

Table: Results for Flight Detectors

SIS position	Micron Semico. Serial No.	junction dead layer (μm)	ohmic dead layer (μm)	junction DL grad. (μm/mm)	ohmic DL grad. (μm/mm)	depletion bias (V)
M1A	008	0.5*	0.5*	<0.01	<0.01	
M2A	022	0.5*	0.5*	<0.01	<0.01	
T1A	P100	0.40	0.31	<0.01	<0.01	10
T2A	016	0.52†	0.34	<0.01	<0.01	10
T3A	119	0.25	0.20	<0.01	<0.01	25
T4A	209	0.26	0.17	<0.01	<0.01	60
T5A	232	0.28	0.30	<0.02	<0.01	60
T6-1A	P1000	0.43†	0.28†	<0.01	<0.01	150
T6-2A	110	0.30	0.17	<0.02	<0.01	140
T6-3A	229	0.24	0.22	<0.01	<0.01	40
T7-1A	221	0.29	0.20	<0.01	<0.01	110
T7-2A	228	0.25	0.15	<0.01	<0.01	100
T7-3A	010	0.38	0.22	<0.01	<0.01	100
T7-4A	125	0.41	0.25	<0.01	<0.01	50
T7-5A	202	0.30	0.23†	<0.01	<0.01	90
T7-6A	204	0.39	0.20	<0.01	<0.01	65
T8A	007	0.24	0.25	<0.02	<0.1	200
M1B	001	0.5*	0.5*	<0.03	<0.03	
M2B	002	0.5*	0.5*	<0.04	<0.03	
T1B	018	0.36†	0.27	<0.01	<0.01	10
T2B	019	0.40	0.47	<0.03	<0.01	10
T3B	023	0.22	0.23	<0.01	<0.03	25
T4B	216	0.33	0.24	<0.01	<0.01	50
T5B	230	0.36	0.20	<0.01	<0.01	55
T6-1B	040	0.30†	0.25	<0.01	<0.01	150
T6-2B	131	0.27†	0.16	<0.03	<0.03	180
T6-3B	214	0.33	0.16	<0.01	<0.01	80
T7-1B	000	0.30	0.17	<0.01	<0.03	175
T7-2B	208	0.31	0.23	<0.01	<0.01	140
T7-3B	126	0.31	0.19	<0.01	<0.01	75
T7-4B	133	0.26†	0.33	<0.01	<0.01	55
T7-5B	200	0.21	0.23	<0.01	<0.01	50
T7-6B	205	0.31	0.15	<0.03	<0.01	70
T8B	103	0.33	0.20	<0.01	<0.01	180

* nominal value

† limits of alpha peaks were set “by hand”, else peaks were automatically found and fit